Generation of Topographic Waves over the Continental Margin

PING-TUNG SHAW AND S. DIVAKAR*

Department of Marine, Earth and Atmospheric Sciences, North Carolina State University, Raleigh, North Carolina

(Manuscript received 5 November 1990, in final form 5 February 1991)

ABSTRACT

Numerical experiments were carried out to simulate the generation of topographic waves by a Gulf Stream ring over the continental margin in a stratified ocean on an f-plane. The study was aimed at understanding the combined effect of density advection and bottom topography on the flow field. The momentum equation is linear, and nonlinearity is introduced in the density equation. The mechanism of wave generation was investigated by turning on and off the nonlinear density advection and by changing the strength of the ring and bottom topography.

The results show that topographic waves are generated by advection of density in a ring over a sloping bottom. The vorticity associated with the swirl velocity of a ring is less important during wave generation. The strength of a ring affects the wave amplitude; in the case of a strong ring, self-advection of density may be induced at the surface. However, the generation and propagation of topographic waves are independent of the strength of the ring. Waves of the observed amplitude can be generated by this process over the continental slope and upper rise off the Mid-Atlantic Bight.

1. Introduction

A common feature along the continental margin off the east coast of North America is the detachment of warm-core rings north of the Gulf Stream, and their subsequent southwestward movement along isobaths (Joyce 1984). A ring may move close to the shelf break and draw off shelf waters onto the slope (Churchill et al. 1986). During the passage of a ring, topographic waves have been observed over the upper slope and the shelf break (Louis et al. 1982; Ramp 1989); thus, the waves are probably generated by the Gulf Stream ring (Louis and Smith 1982). Observations also show that topographic waves dominate the near-bottom kinetic energy spectrum on the lower slope (Shaw and Csanady 1988). Some wave energy may come from the meandering Gulf Stream (Hogg 1981), but it may also be generated locally by rings. Since the continental slope off the Mid-Atlantic Bight is a region of low kinetic energy (Csanady and Shaw 1983; Csanady et al. 1988), topographic waves generated locally by the Gulf Stream ring may dominate the energy spectrum.

Despite the observational evidence of a possible relationship between topographic waves and the passage

of a ring, the process of wave generation on the continental slope is not known. In models of topographic waves, forcing is usually specified in the vorticity equation without considering the mechanism of wave generation. For example, Louis and Smith (1982) studied the topographic wave field generated by a vorticity source on the slope in a homogeneous ocean and concluded that the observed currents are consistent with the calculated wave field. Shaw and Peng (1987) used a similar approach to study the energy of topographic waves over the continental margin. Their results show that the onshore propagation of topographic wave energy is blocked by the steep slope, but waves generated locally on the slope are trapped. Although these studies shed light on the propagation of topographic waves, how waves are generated by a ring has not been investigated.

The effect of a ring on currents over the continental margin has been simulated by specifying a localized pressure distribution along the offshore boundary in both a continuously stratified model (Chapman and Brink 1987) and a two-layer model (Qiu 1990). Although density stratification is present in these models, there is no nonlinear advection of density. The results of Chapman and Brink show that motion induced by a ring on an f-plane decays in a scale of the first baroclinic Rossby radius of deformation. Thus, there is little energy reaching the slope unless the ring is nearby. Qiu included the beta effect in his model, so that there are baroclinic waves propagating toward the coast. His results indicate that currents on the shelf and slope are affected only under resonance conditions. Thus, to-

* *Present affiliation:* Center for Atmospheric Science, Indian Institute of Science, Bangalore 560012, India.

Corresponding author address: Dr. Ping-Tung Shaw, Dept. of Marine, Earth and Atmospheric Sciences, North Carolina State University, Box 8208, Raleigh, NC 27695-8208

pographic waves on the upper slope are not generated by eddies away from the slope.

Topographic waves over the continental margin are either barotropic or bottom intensified (Thompson and Luyten 1976; Hogg 1981), so sources are likely to be located near the bottom. Since a stable ring in a two-layer ocean tends to evolve to a compensated state without bottom flow (e.g., McWilliams and Flierl 1979; Mied and Lindemann 1979), a ring in a quasi-steady state in the upper layer does not feel bottom topography, and little energy radiates away as topographic waves. Topographic waves can be generated only if there is a lower-layer circulation in a ring (Smith 1986). Such a deep circulation can be produced by adjustment of the velocity field to the density structure in a process similar to the Rossby adjustment problem (Gill 1982). This process is initiated if a ring is not in geostrophic balance. Large-amplitude ageostrophic motions are common during the meandering of the Gulf Stream front and the detachment of a Gulf Stream ring. The bottom circulation generated by the adjustment process in a ring is a source of vorticity for topographic waves.

Bottom forcing may also come from nonlinear advection of density over topography when a ring is close to the shelf break. Csanady (1988) has shown that the pressure torque term in the vorticity equation may become large enough to generate topographic waves during the pinching off of Gulf Stream rings. Although the process was not fully investigated, his study suggested that large-amplitude variation in the depth of isopycnals in a ring and bottom slope are essential for the wave generation. In this paper, the mutual adjustment of the density and velocity fields in a ring is studied in the context of topographic wave generation. The results show that topographic waves are generated more efficiently by nonlinear advection of density than by the vorticity associated with the swirl velocity of a ring.

The problem was solved using the semi-spectral primitive equation model (SPEM) developed by Haidvogel et al. (1991). The model has been applied successfully to a seamount problem with a steep bottom topography (Haidvogel, personal communication, 1990). In this paper, the bottom topography and the mean stratification are similar to those in the slope-rise region off the Mid-Atlantic Bight.

2. Model formulation

In order to have a clear understanding of the dynamics, we have kept only the essential terms in the model equations. Since our hypothesis is that topographic waves are generated by density advection, the nonlinear terms in the density equation are retained. However, because of the weak current in the deep layers of a ring, the nonlinear terms in the momentum equation are neglected. Furthermore, it is not our intention to study the propagation of isolated eddies, so the Co-

riolis parameter f is a constant equal to 10^{-4} s^{-1} in this paper. We will show later that the Rossby number is small in all cases considered. Therefore, the process of wave generation, which has a time scale of a few days, is not affected by nonlinear momentum advection. The model geometry is a periodic channel in the
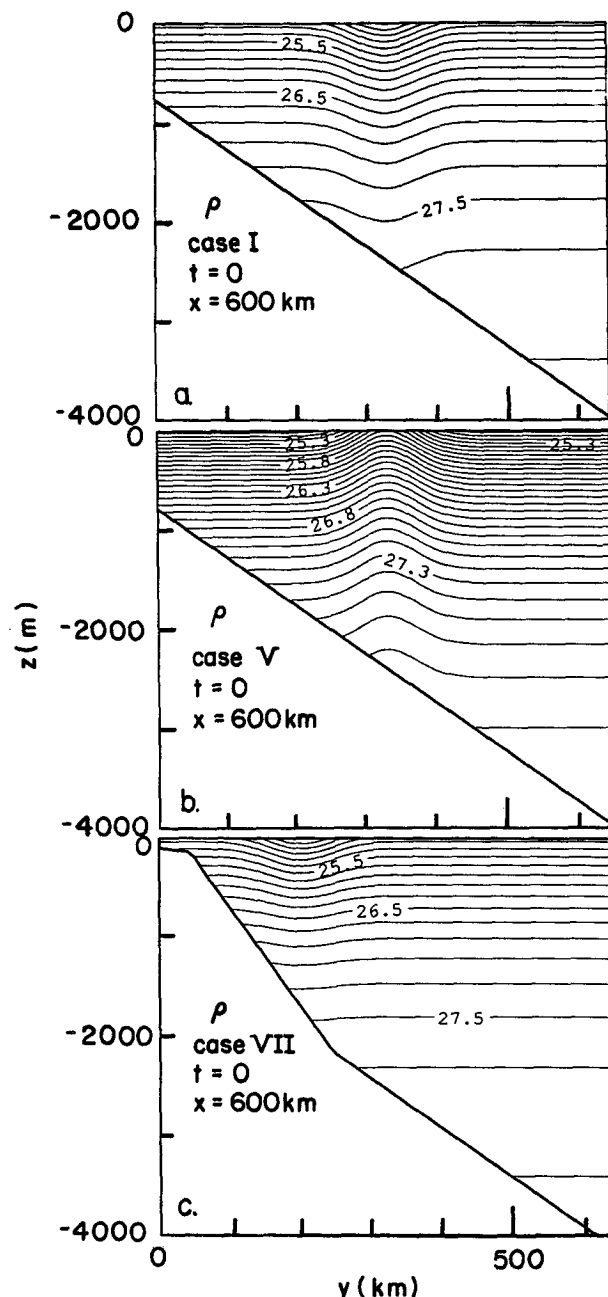

FIG. 1. Initial density distribution in units of kg m^{-3} in the cross-isobath section through the center of the ring: (a) cases I, II and VI; (b) Case V; and (c) cases III and VII. The bottom topography is a constant slope of 0.005 in (a) and (b) and a slope-rise topography in (c). The contour interval is 0.2 in (a) and (c) and is 0.1 in (b).

TABLE 1. Summary of cases studied.

| | Topography at ring location | | | Density structure ρ_{max} at $t = 0$ | | | |
| | | | | | 100 m | 2000 m | |
Case	slope	depth (m)	b (m)	q (kg m⁻³)	(kg m⁻³)		Comments
I	0.005	2400	1000	−1	0.905	0.135	
II	0.005	2400	1000	−1	0.905	0.135	diagnostic
III	0.005	2400	500	−1	0.819	0.018	
IV	0.005	2400	1000	−2	1.81	0.270	
V	0.005	2400	1000	+1	0.905	0.135	cold-core ring
VI	0	2400	1000	−1	0.905	0.135	flat-bottom
VII	0.01	1650	500	−1	0.819	0.018	slope-rise topography

x-direction with y and z representing the cross-channel and upward coordinates, respectively. The origin of the coordinate system is at the lower left corner of the channel, and $z = 0$ is at the surface. The corresponding velocity components are u, v and w. With the hydrostatic approximation, the linear momentum equation is

$$\frac{\partial u}{\partial t} - fv = -\frac{1}{\rho_0}\frac{\partial p}{\partial x} \qquad (1a)$$

$$\frac{\partial v}{\partial t} + fu = -\frac{1}{\rho_0}\frac{\partial p}{\partial y} \qquad (1b)$$

$$0 = -\frac{\partial p}{\partial z} - \rho g \qquad (1c)$$

where t is time; $g = 9.8$ m s⁻² is the gravitational constant; $\rho_0 = 1000$ kg m⁻³, a constant reference density; and p and ρ are the perturbation pressure and density, respectively. The continuity equation is

$$\frac{\partial u}{\partial x} + \frac{\partial v}{\partial y} + \frac{\partial w}{\partial z} = 0 \qquad (2)$$

while the advection of density is given by

$$\frac{\partial \rho}{\partial t} + u\frac{\partial \rho}{\partial x} + v\frac{\partial \rho}{\partial y} + w\frac{\partial \rho}{\partial z} = \frac{\rho_0}{g}N^2w \qquad (3)$$

where $N^2 = -(g/\rho_0)d\bar{\rho}/dz$, and $\bar{\rho}(z)$ is the mean stratification. Vertical advection of density perturbation is kept in (3) because of the large-amplitude variation in the depth of isopycnals in a Gulf Stream ring. The same equations without vertical density variation in (3) and time-dependence in (1) have been used by Shaw and Csanady (1983) to demonstrate the self-advection of density perturbation on a vertically mixed, sloping continental shelf.

The length of the channel is 1470 km, and the width is 640 km. The grid size is 30 km by 10 km. The isobaths are parallel to the channel walls, and the bottom depth increases in the positive y-direction. In the nu-

merical calculation, there are three types of bottom topography. The first consists of a constant slope of 0.005, typically found on the upper rise (Fig. 1a). The mean depth is 2400 m. The second has a constant depth of 2400 m. The third is similar to that over the continental margin: a shelf, a slope and a rise with bottom slopes of 0.001, 0.01 and 0.005, respectively. The shelf is 50 km wide, with a depth varying from 100 m at the coast to 150 m at the shelf edge. Off the shelf break is a narrow slope 200 km wide with depth increasing to 2150 m. The bottom of the deep ocean is at 4000 m. A cross section of the topography is shown in Fig. 1c.
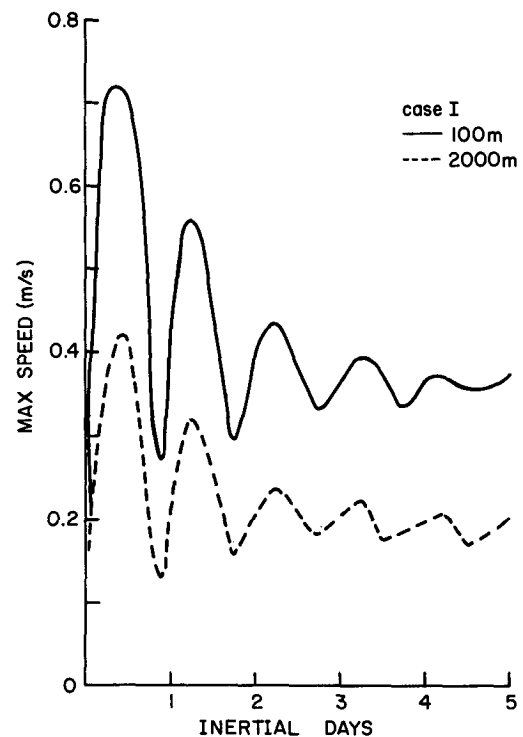

FIG. 2. Maximum current speeds at 100 m (solid line) and at 2000 m (dashed line) in Case I during the first five inertial cycles.
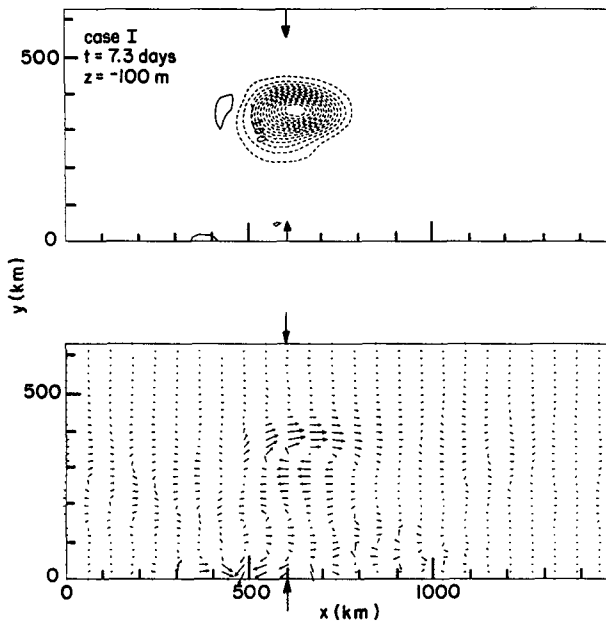
FIG. 3a. Distributions of perturbation density and velocity at 100 m in Case I after 10 inertial cycles (7.3 days). The density contours in kg m^{-3} are from -0.6 to 0 with an increment of 0.04. Dashed contours represent negative perturbation density. The velocity vector is plotted every 60 km in x and 20 km in y. The maximum velocity vector is 0.29 m s^{-1}. The initial location of the ring is at 600 km, indicated by a set of arrows.

The mean stratification in units of kg m^{-3} is given by $\bar{\rho}(z) = 28.0 - 3.0 \exp(z/1000)$ with the depth z in meters. The initial density distribution is

$$\rho = q \exp\left(\frac{z}{b}\right) \exp\left[-\frac{(x^2 + y^2)}{a^2}\right] \qquad (4)$$

where q is the density perturbation at the center of the ring; negative (positive) q represents a warm-core (cold-core) ring. The horizontal and vertical scales of the ring are a and b, respectively. Equation (4) provides a simple mathematical description of the observed vertical displacement of isopycnals in a ring (Joyce 1984). Since our concern is the effect of bottom topography on deep currents, the structure of the ring at shallow depths will not alter the results significantly. In the model, the strength of the ring is varied by changing q and b. A strong warm-core ring with a density perturbation reaching the bottom is used in cases I, II and VI (Fig. 1a). The ring in Case V is a cold-core version of this one (Fig. 1b), and that in cases III and VII (Fig. 1c) has a more realistic stratification with a vertical e-folding scale one-half of that in Fig. 1a. Finally, the density deficit of the ring in Case IV is twice that in Fig. 1a (not shown). A summary of the ring parameters is given in Table 1. In case I, the first baroclinic Rossby radius of deformation, calculated from the maximum value of N at the surface and a mean depth $H = 2400$

m, is 42 km, which is less than the ring diameter, 120 km, in this paper. We have also used a larger ring of a diameter of 240 km, but the results are not qualitatively different.

The evolution of the flow and density fields was obtained by integrating (1)–(3) in time from an initial state of no motion. The time step of integration was 785 sec, which is 1/80 of the inertial period in this study. The rigid-lid approximation was used; thus, surface gravity waves were filtered out. At the bottom and sidewalls, there was neither momentum flux nor density flux through the boundary. In the numerical calculation, a biharmonic friction with a coefficient, 8.0 $\times$ 10^9 m^4 s^{-1}, was applied to (1), and the density field was smoothed with a Sharpiro filter. The vertical structure was represented by seven spectral modes in terms of Chebyshev polynomials. A detailed description of the computer program was given by Hedström (1989).

3. Results

a. Ring on the continental rise

The ring in Case I is on a moderate bottom slope of 0.005. The first response of the fluid to the initial density perturbation is to generate inertial oscillations, as shown in the time-series plot of the maximum speed in the ring (Fig. 2). The maximum speed reached a quasi-steady state after a few inertial cycles and so did
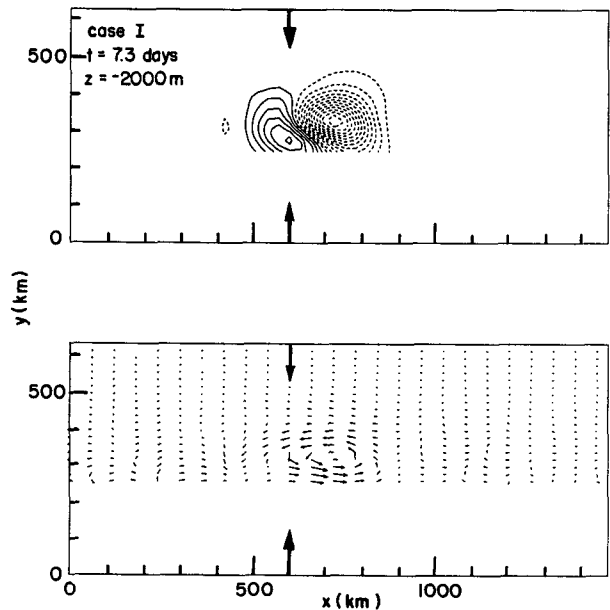

FIG. 3b. As in (a) but at 2000 m. The density contours are from -0.12 to 0.05 with an increment of 0.01. The maximum velocity vector is 0.17 m s^{-1}.
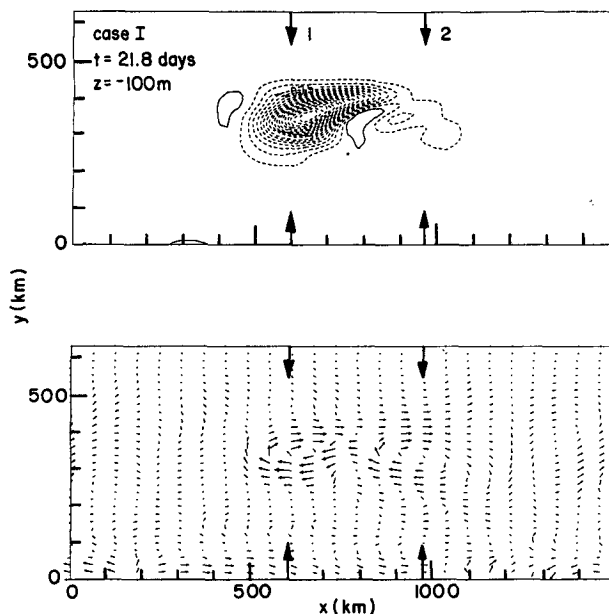
FIG. 4a. Same as Fig. 3 except at $t = 21.8$ days and $z = -100$ m. Contour lines are from -0.54 to 0 with an interval of 0.03. The maximum velocity vector is 0.22 m s^{-1}.

the density. The density structure at 100 m at the end of 7.3 days (10 inertial cycles) was similar to the initial structure at the same depth, except for a smaller density deficit (Fig. 3a, upper panel). There was weak nonlinear advection of density as indicated by the small offshore movement of the ring center. The current at 100 m was anticyclonic with a maximum speed of 0.29 m s^{-1} (Fig. 3a, lower panel). Gravity waves propagated away from the ring and were intensified in shallow waters, but the density field was not affected by gravity waves. At 2000 m, a cyclonic circulation developed and moved toward the positive x-direction (Fig. 3b, lower panel). The circulation at the bottom was only about half the strength of the current at 100 m but was crucial to the development of a deep density perturbation. The bottom topography prevented the formation of a steady deep cyclone. Continuity resulted in upward motion at the location of onshore flow and downward motion at that of offshore flow. The density advection by the vertical velocity created a dipole at the bottom (Fig. 3b, upper panel).

Both the density perturbation and the velocity were nonstationary. At $t = 21.8$ days (30 inertial cycles), the center of the surface eddy was advected slightly to the right, and the density contours were distorted (Fig. 4a). In the velocity field, an anticyclone was associated with the surface density structure of the ring as at $t = 7.3$ days, but another anticyclone developed to the right of the ring. The surface density field was only slightly affected by the second anticyclone because of the weak vertical velocity at shallow depths under the

rigid-lid approximation. At 2000 m (Fig. 4b), the center of the eddy was 360 km to the right of its initial location. Behind the eddy were several weaker ones in the density field. The deep cyclone followed the movement of the main eddy and was intensified on the shallow water side. Outside the deep eddy, the current was weak. In the vertical cross-isobath section through the center of the ring (Fig. 5a), both the density perturbation and velocity decayed rapidly toward the bottom; the ring had evolved to a compensated state. In the meantime, the density structure of the propagating eddy was intensified at the bottom, and a surface anticyclone was on top of a bottom cyclone (Fig. 5b). The velocity structure was of a first baroclinic mode.

The density perturbation propagates much faster at the bottom than at the surface (Fig. 6). From the location of the center of the deep eddy, the propagation speed at the bottom is estimated to be 0.19 m s^{-1}. The maximum particle speed in Fig. 5b is 0.20 m s^{-1}, too small to advect the bottom density perturbation as a Lagrangian eddy. It is more likely that the propagation is associated with a wave front similar to that in the Rossby adjustment problem. In an f-plane, flat-bottom ocean, inertial gravity waves propagate away from an initial perturbation (Gill 1982). However, the group velocity of the first baroclinic gravity waves, $NH/\pi = 4.2$ m s^{-1} ($H = 2400$ m) is much higher than the propagation speed of the density perturbation in Case I. Thus, the propagation of the deep density perturbation is not due to gravity waves.

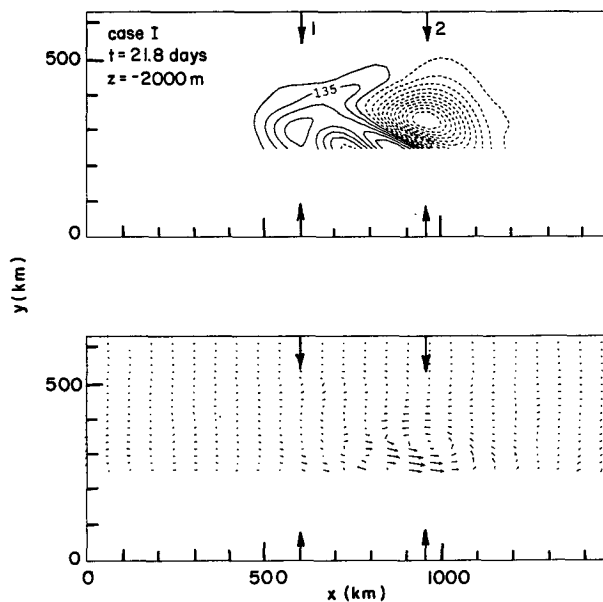The Rossby number is small in this case. A length scale of 120 km, which is the diameter of the ring, and

FIG. 4b. As in (a) but at 2000 m. Density contours are from -0.099 to 0.045 with an interval of 0.009. The maximum velocity vector is 0.19 m s^{-1}.
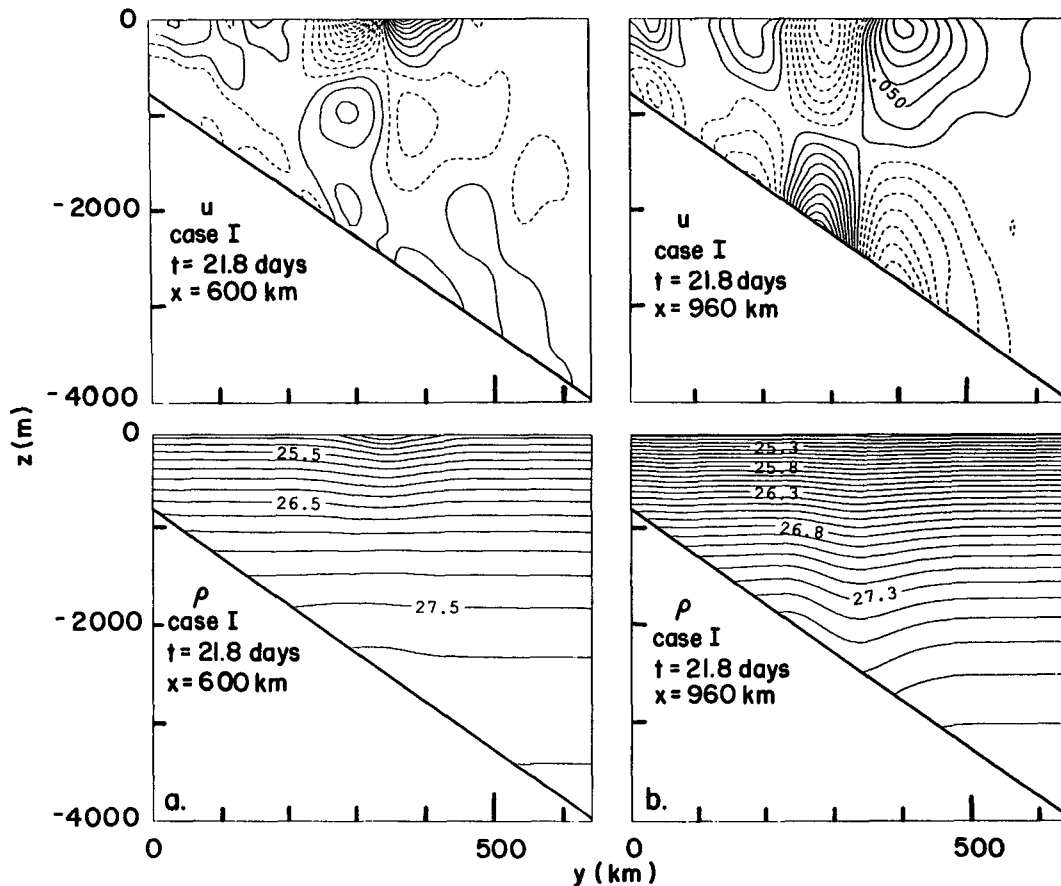
FIG. 5. Contour lines of u (upper panels) and density (lower panels) in the z-y plane at $t = 21.8$ days in Case I: (a) at section 1 and (b) at section 2. The locations are shown in Figs. 3 and 4. The velocity contours are from -0.24 to 0.16 m s^{-1} in (a) and from -0.14 to 0.2 m s^{-1} in (b). In both sections, the contour interval is 0.02 m s^{-1}. Negative u is represented by dashed lines. Contour intervals for density are 0.2 and 0.1 in (a) and (b), respectively.

a velocity scale of 0.4 m s^{-1} give a Rossby number 0.03 at 100 m. The velocity is weaker at the bottom, so the bottom Rossby number is even smaller. Therefore, the momentum equation is governed by quasigeostrophic dynamics. The result justifies the neglect of the nonlinear terms in the momentum equation. In such a dynamic regime, the propagation of density perturbation in Fig. 4b is induced by topographic waves. In an equivalent case on a beta-plane, Rossby waves propagate away from a weak buoyancy source in a reduced-gravity model (Davey and Killworth 1984). Since long topographic waves have the highest group velocity along isobaths, the propagation is associated with these nondispersive waves. We will show in section 4 that the propagation speed of the bottom cyclone is equal to the phase speed of nondispersive topographic waves. During wave propagation, nonlinearity in the momentum equation is probably important: the particle speed at the bottom is comparable to the phase speed of topographic waves. However, wave propagation is not the primary concern of this paper.

b. Diagnostic calculation

In Case I, a bottom cyclone developed at the end of the initial adjustment and propagated away from the ring. The swirl velocity associated with the cyclone is a possible source of vorticity for the generation of topographic waves. A vorticity source is common in the study of propagation of topographic waves in barotropic models (Louis and Smith 1982; Shaw and Peng 1987). In order to find the effect of a vorticity source on wave generation, we have solved (1) and (2) without the density equation (3) (Case II). In such a diagnostic calculation, the ring structure does not evolve with time.

Similar to Case I, an anticyclone developed at the surface after a few inertial cycles. A cyclone formed at the bottom, but there was no dipole structure in the density field. The maximum swirl speeds of the cyclone changed little afterward and were about twice that in Case I (Table 2). Without density advection, the deep cyclone remained at its initial location (Fig. 7). There
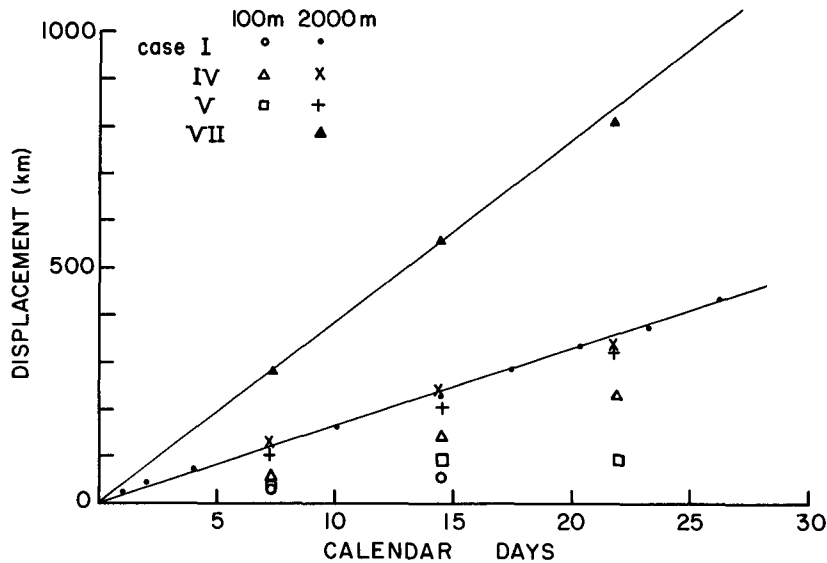
FIG. 6. Location of the center of the density perturbation as a function of time.

was no evidence of topographic waves, and energy was radiated away from the ring only by weak inertial gravity waves. The difference in kinetic energy between cases I and II indicates that the energy loss in Case I was due to the radiation of topographic waves. The diagnostic result shows the importance of nonlinear density advection in wave generation.

c. Rings of varying strength

The effect of nonlinearity in the density equation is further investigated on the same topography in cases III–V. First the vertical scale of the initial density structure of the ring is reduced to 500 m (Case III). The initial density deficit at the surface is similar to that in Case I, but the bottom density perturbation is smaller (Table 1). After 7.3 days, the density deficit at

TABLE 2. Magnitude of the maximum density perturbation and particle speed.

	Maximum ρ (kg m^{-3})				Maximum speed (m s^{-1})			
	100 m		2000 m		100 m		2000 m	
			Day					
Day Case	7	14	7	14	7	14	7	14
I	0.6	0.57	0.12	0.11	0.29	0.21	0.17	0.18
II	0.68	0.64	0.102	0.096	0.63	0.61	0.32	0.32
III	0.57	0.54	0.036	0.036	0.20	0.16	0.06	0.05
IV	1.2	1.12	0.22	0.22	0.57	0.41	0.33	0.31
V	0.54	0.48	0.13	0.13	0.36	0.25	0.25	0.18
VI	0.6	0.6	0.08	0.075	0.38	0.31	0.17	0.15
VII	0.57	0.54	0.04	0.028	0.14	0.16	0.13	0.08

100 m was not different from that in Case I, but the maximum speed was 30% less (Table 2). Despite the weaker flow, an anticyclone developed at the surface (not shown), but the surface density field was much less distorted by density advection than in the previous case. At 2000 m, both the maximum density deficit and maximum speed were one-third of the corresponding values in Case I (Table 2). Nevertheless, a dipole structure formed at the bottom, and a cyclone propagated at the same speed as that in Case I. The maximum density perturbation at 2000 m depended on the strength of the ring and was about twice its initial value after 7.3 days in Case III (Tables 1 and 2). The increase in magnitude of the density perturbation indicates that the dipole is formed by vertical density advection induced by cross-isobath flow over a sloping bottom. Except for a smaller amplitude, waves are generated by a weaker ring.

The ring in Case IV has the same vertical scale as that in Case I, but the maximum density deficit is doubled. At 7.3 days, the maximum speed at 100 m was twice that in Case I, and so was the bottom velocity (Table 2). The surface density structure was stretched toward the direction of topographic wave propagation, and another ring center formed (Fig. 8). The Rossby number, 0.05, is still small, but the nonlinear advection of the density field is much stronger than in Case I. Nevertheless, the original density structure of the ring at 100 m can still be identified at its initial location. The propagation speed of the new ring center is less than that of topographic waves (Fig. 6). The stronger density advection is a result of the higher current speed at the propagating wave front. At the bottom, the particle speed was about twice the phase speed, but the
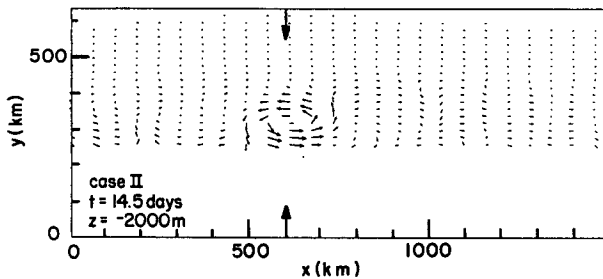
FIG. 7. Same as Fig. 3 except for velocity at $z = -2000$ m and t = 14.5 days in Case II. The maximum vector is 0.32 m s^{-1}.

nonlinearity did not appear to affect the propagation speed of the wave front (Fig. 6). The larger initial density deficit in the ring produces a stronger wave front, but the current and density fields are not qualitatively different from those in cases I and III. Thus, the strength of the ring affects the amplitude of the topographic wave but not the process of wave generation.

The ring in Case V has a density surplus instead of density deficit, representing a cold-core ring. The major difference between cases V and I is in the density advection at the surface. The surface density field was advected farther toward the positive x-direction than in Case I (Figs. 6 and 9). In addition, density contours were stretched toward the negative y-direction; the center of the deep eddy was closer to the slope than in Case I. The cross-isobath density advection is equivalent to the northward movement of a cyclone on the beta plane, as observed by Davey and Killworth (1984) in a reduced-gravity model of dynamics similar to (3). In a two-layer ocean with a sloping bottom, Smith (1986) also found that cyclones are more likely to propagate onto the continental shelf than anticyclones. Nevertheless, the process of wave generation is not affected significantly by nonlinear self-advection, as shown by the same propagation speed of bottom density perturbation (Fig. 6).

d. Ring on a flat bottom

The effect of bottom slope on the formation and propagation of density perturbation is examined in Case VI. The ring has the same structure as in Case I but is in an ocean of a constant depth of 2400 m, the water depth at the ring location in earlier cases.

The maximum particle speed at 2000 m after 7.3 days is similar to that in Case I (Table 2). Thus, the adjustment of the velocity field to an initial density perturbation is not affected by bottom slope. The density perturbation at the surface is also similar in both cases (Table 2). The most significant difference is the absence of a dipole at the bottom in Case VI, although the initial density deficit is of the same magnitude in both cases. Without topography, a cyclone at the bottom can exist indefinitely, and no vorticity waves

propagate away from the ring (not shown). Less energy is lost from the ring as indicated by a higher speed at 100 m than in Case I (Table 2). Case VI shows that the formation of a dipole is a result of density advection induced by vertical motion on a sloping bottom.

e. Ring on the continental slope

In case VII, we have used slope-rise topography similar to that off the Mid-Atlantic Bight (Fig. 1c). The imposed density structure, centered at $y = 200$ km, is the same as in Case III. The response of the density and velocity fields is similar to that in Case III: at the end of 21.8 days the surface density structure was not significantly different from that at $t = 0$, and an anticyclone formed at 100 m (Fig. 10). However, the propagating wave front was farther to the right. The propagation speed of the wave front was about twice that in cases I and III (Fig. 6) as a result of the slope being twice as steep. The ring evolved to a compensated state with weak bottom flow as in Case I (Fig. 11a). Similarly, the density perturbation associated with the propagating wave front was intensified at the bottom, as shown by the tilting isopycnals at the bottom of the slope (Fig. 11b). The wave front is confined by the steep bottom slope in this case.

The increase in the propagation speed is due to the higher group velocity of topographic waves. For nondispersive topographic waves, the phase speed increases with the bottom slope, and so does the group velocity. Despite the higher propagation speed, the particle speed at the wave front is similar in cases III and VII at the end of 14 days (Table 2). Thus, the magnitude of the bottom slope affects the propagation speed of density perturbation but not the amplitude. The along-isobath velocity component is of the order of 0.1 m s^{-1}, which is the typical amplitude of topographic waves observed on the slope (Louis et al. 1982).

4. Discussion

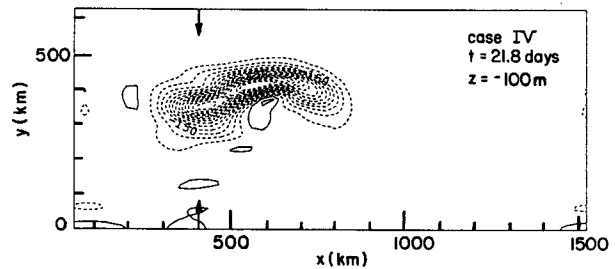Louis and Smith (1982) found that the swirl speed in their model has to be one order of magnitude higher

FIG. 8. Same as Fig. 3 except for perturbation density at $z = -100$ m and $t = 21.8$ days in Case IV. The ring is initially at $x = 400$ km. Contour lines are from -0.9 to 0.06 with an increment of 0.06.
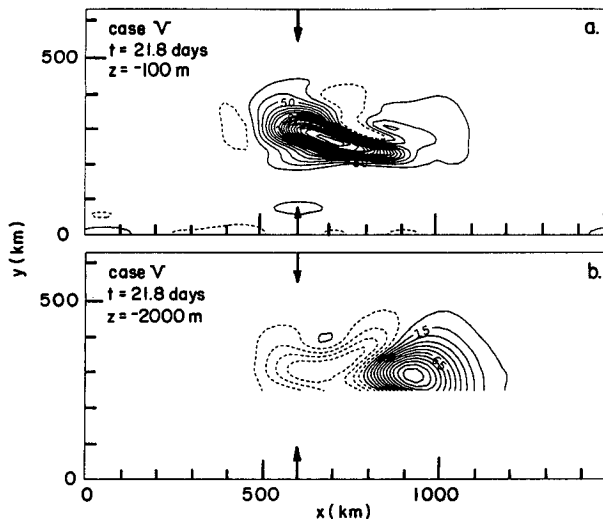
FIG. 9. Same as Fig. 3 except for perturbation density at $t = 21.8$ days in Case V: (a) 100 m and (b) 2000 m. The contours are from -0.02 to 0.38 with an increment of 0.02 in (a) and are from -0.04 to 0.12 with an increment of 0.01 in (b).

than that in the ocean in order to generate waves of the observed amplitude. Their model is barotropic; thus, it is equivalent to the diagnostic model of Case II. The result of Case II shows that the vorticity associated with the velocity field at the bottom is not an effective source of topographic waves. The absence of density advection explains why a strong vorticity source is needed. This is also the case when the bottom layer of a two-layer ocean is deep; there is no significant propagation of density perturbation along bottom contours even when there is a deep circulation (Smith 1986). Equally important to the wave generation is the presence of a steep bottom slope. Without bottom topography, there is little density advection because of the lack of vertical motion at the bottom. A bottom cyclone can exist indefinitely; little energy radiates away from the ring. Strong vertical density advection occurs only when there are both a steep bottom slope and a large variation in the depth of isopycnals. Thus, the advection of density over a sloping bottom is the mechanism of wave generation.

Cross-isobath currents of the order of 0.1 m s^{-1} have been observed in the deep Gulf Stream off Cape Hatteras by Johns and Watts (1985). The deep currents are highly coherent with the movement of the Gulf Stream front, and the density balance is described by (3). Although the density perturbation is weaker in a ring than at the Gulf Stream front, the balance in (3) may still hold because of stronger vertical motion induced by a steeper bottom topography. Thus, the dynamics proposed in this paper can exist in the ocean. The numerical results show that the topographic wave generated by this process is of the correct order of magnitude as observed.

Density advection over a sloping bottom is essential in the self-advection process of Shaw and Csanady (1983). On a continental shelf without vertical density variation, along-isobath currents are induced by divergence and convergence of horizontal flow on a sloping bottom. The nonlinear interaction between the along-isobath current and density produces self-advection. The present study generalizes the two-dimensional process to include vertical density stratification. Vertical advection of density over a sloping bottom generates density perturbation propagating away from a ring in the form of topographic waves. Although the momentum equation in this model is quasi-geostrophic, the existence of vertical advection of perturbation density makes the present formulation different from a quasi-geostrophic model. Nonlinear advection may contribute to the different propagation speeds of an eddy in a quasi-geostrophic model and in a primitive-equation model when there is large variation in the depth of isopycnals (Davey and Killworth 1984).

The model suggests a mechanism of generating topographic waves by a Gulf Stream ring. The process is initiated by ageostrophy in a ring. In the ocean, ageostrophic motion may develop during the formation of a ring, meandering of the Gulf Stream path, and the shoaling of a ring on the slope. Instability may also induce ageostrophic motion. Recent study by Paldor and Nof (1990) shows that a ring may become unstable when it moves to shallow waters. We are not concerned about the development of ageostrophic motion in this paper. Nevertheless, once a ring is not in geostrophic
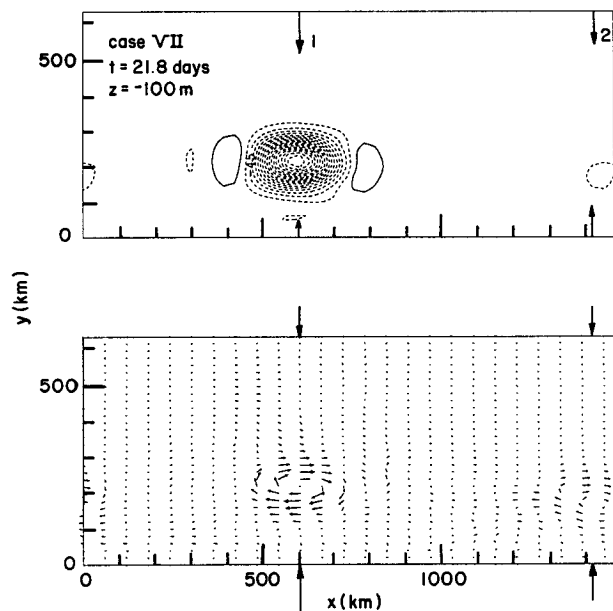

FIG. 10. Same as Fig. 3 except at $z = -100$ m and $t = 21.8$ days for Case VII. Density contours are from -0.51 to 0.03 with an increment of 0.03. The maximum velocity vector is 0.14 m s^{-1}.
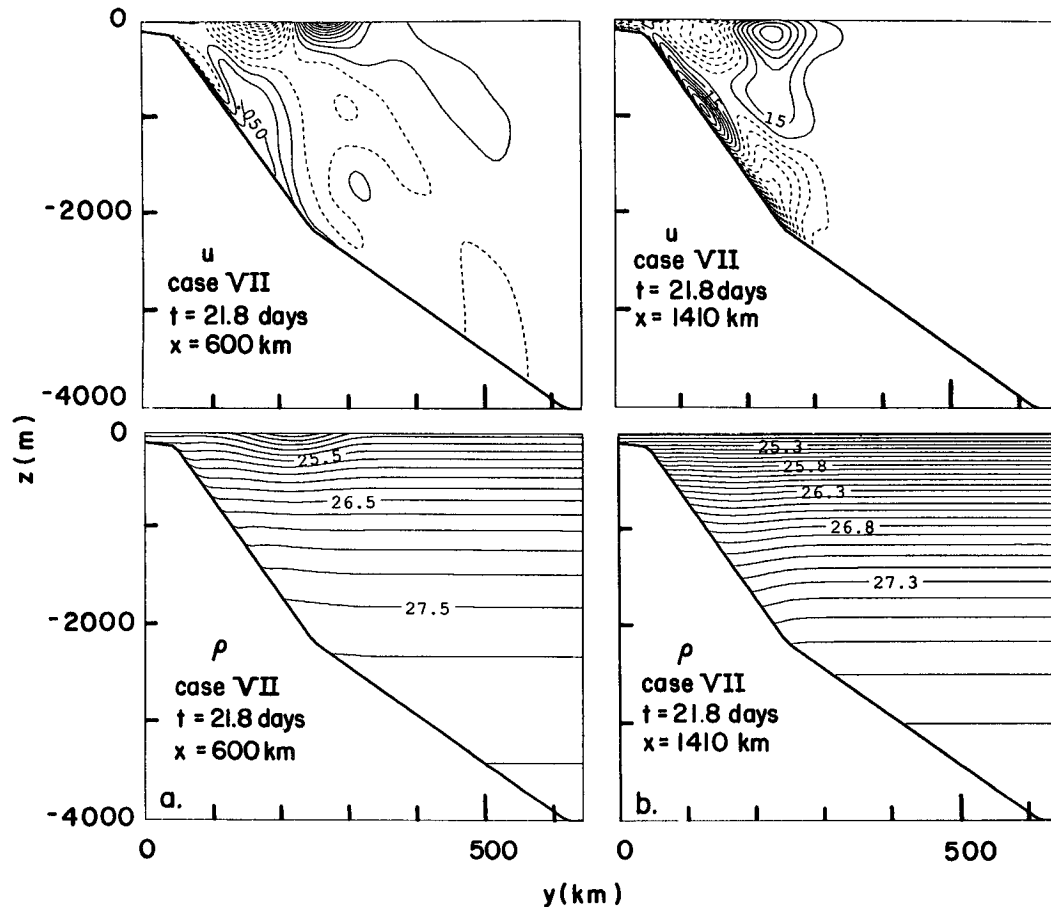
FIG. 11. Same as Fig. 5 except for Case VII: (a) at section 1 and (b) at section 2. The locations are shown in Fig. 10. The contours for u are from -0.2 to 0.2 with an interval of 0.02 m s^{-1} in (a) and from -0.14 to 0.07 with an interval of 0.01 m s^{-1} in (b). The contour interval for density is 0.2 in (a) and 0.1 in (b).

balance, topographic waves are generated. Radiation of wave energy stops when a ring reaches a steady, compensated state without bottom flow (Smith 1986). A consequence of this process is that topographic waves are probably generated intermittently. The intermittent nature of topographic wave oscillation is commonly observed in the ocean. For example, Louis et al. (1982) reported four events of topographic wave oscillations over one year, each event lasting for only three or four cycles. Similarly, Price and Rossby (1982) found Rossby wave oscillation of two and a half cycles in the SOFAR float trajectories to the southwest of Bermuda.

In the parameter range of this paper, the propagation speed of the bottom density perturbation depends only on the bottom slope, not on the strength of the ring or the sign of the density perturbation. With a cross-isobath scale of 200 km, the phase speed of long topographic waves is 0.2 m s^{-1} on a bottom slope of 0.005 in a homogeneous ocean 2000 m deep. This value is comparable to the speed on the rise in Fig. 6. With a bottom slope twice as steep, the theoretical phase speed

is 0.4 m s^{-1}, close to the propagation speed of the bottom density perturbation on the continental slope. The waves are not monochromatic but in the form of a wave front, which is typical in the Rossby adjustment problem (Gill 1982). Furthermore, the wave front is trapped by the slope topography as in a homogeneous ocean (Shaw and Peng 1987). The propagation of the wave front is not significantly affected by stratification.

The Burger number, which is the square of the ratio of the internal Rossby radius of deformation to the length scale, is small in all cases considered in this paper. Therefore, it is not surprising that the speed of propagation of density perturbation at the bottom agrees with barotropic theory. However, the current structure at the wave front is not barotropic. Examination of the density and velocity fields shows that the velocity shear and the horizontal density gradient are approximately in thermal-wind balance. The result is consistent with the small Rossby number in the model; the velocity is approximately in geostrophic balance. The geostrophic velocity consists of two components:

a baroclinic component relative to the bottom and a barotropic component. The barotropic component is associated with the propagation of topographic waves and is not greatly affected by stratification. On the other hand, the baroclinic component reflects the density structure of the propagating density perturbation but is not important to the wave propagation.

It is possible that the propagation of density perturbations at the bottom is due to dynamics governing the motion of an isolated eddy. The translation speed of an isolated eddy on a sloping bottom has been derived by Nof (1985). The propagation speed of a deep-ocean eddy is given by $g(\rho/\rho_0)\alpha/f$, where the notation in this paper has been used and α is the bottom slope. According to this formula, the propagation speed is 0.12 m s^{-1} on the slope (Case VII) and 0.06 m s^{-1} on the rise (Case I). These values are only one-third to one-fourth of the values obtained in Fig. 6. The result is not surprising. The ring in Nof's paper is strong, and the pressure force is balanced by the centrifugal force as well as the Coriolis force; the centrifugal force is negligible in all cases considered in this paper. Therefore, the propagation is not explained by translation of an isolated eddy.

5. Summary and conclusion

Topographic waves were generated during the mutual adjustment of the velocity field and the density structure of a ring over a sloping bottom. The adjustment process produced a cyclone (anticyclone) at the bottom in the case of a warm-core (cold-core) ring, and vertical motion was induced by convergence and divergence of the bottom circulation over topography. Density advection by the vertical velocity then generated topographic waves. Since the process is initiated when the density and the velocity fields in a ring are not in geostrophic balance, the process may explain why topographic waves observed in the ocean are intermittent. Density stratification is important during wave generation, but wave propagation can be explained by barotropic theory. The results show that topographic waves of the observed amplitude can be generated by a Gulf Stream ring on the continental rise and slope. Thus, the Gulf Stream ring is an efficient source of topographic waves off the Mid-Atlantic Bight.

REFERENCES

Chapman, D. C., and K. H. Brink, 1987: Shelf and slope circulation induced by fluctuating offshore forcing. *J. Geophys. Res.,* **92,** 11 741–11 759.

Churchill, J. H., P. C. Cornillon and G. W. Milkowski, 1986: A cyclonic eddy and shelf–slope water exchange associated with a Gulf Stream warm-core ring. *J. Geophys. Res.,* **91,** 9615–9623.

Csanady, G. T., 1988: Radiation of topographic waves from Gulf Stream Meanders. *Contin. Shelf Res.,* **8,** 673–686.

——, and P.-T. Shaw, 1983: The "insulating" effect of a steep continental slope. *J. Geophys. Res.,* **88,** 7519–7524.

——, J. H. Churchill and B. Butman, 1988: Near-bottom currents over the continental slope in the Mid-Atlantic Bight. *Contin. Shelf Res.,* **8,** 653–671.

Davey, M. K., and P. D. Killworth, 1984: Isolated waves and eddies in a shallow water model. *J. Phys. Oceanogr.,* **14,** 1047–1064.

Gill, A. E., 1982: *Atmosphere-Ocean Dynamics,* Academic Press, 662 pp.

Haidvogel, D., J. Wilkin and R. Young, 1991: A semi-spectral primitive equation ocean circulation model using vertical sigma and orthogonal curvilinear horizontal coordinates. *J. Comput. Phys.,* in press.

Hedström, K. S., 1989: User's manual for a semi-spectral primitive equation regional ocean-circulation model, Version 2.0. unpublished manuscript, 86 pp.

Hogg, N., 1981: Topographic waves along 70°W on the continental rise. *J. Mar. Res.,* **39,** 627–649.

Johns, W. E., and D. R. Watts, 1985: Gulf Stream meanders: observations on the deep currents. *J. Geophys. Res.,* **90,** 4819–4832.

Joyce, T. M., 1984: Velocity and hydrographic structure of a Gulf Stream warm-core ring. *J. Phys. Oceanogr.,* **14,** 936–947.

Louis, J., and P. C. Smith, 1982: The development of the barotropic radiation field of an eddy over a slope. *J. Phys. Oceanogr.,* **12,** 56–73.

——, B. Petrie and P. Smith, 1982: Observations of topographic Rossby waves on the continental margin off Nova Scotia. *J. Phys. Oceanogr.,* **12,** 47–55.

McWilliams, J. C., and G. R. Flierl, 1979: On the evolution of isolated, nonlinear vortices. *J. Phys. Oceanogr.,* **9,** 1155–1182.

Mied, R. P., and G. J. Lindemann, 1979: The propagation and evolution of cyclonic Gulf Stream rings. *J. Phys. Oceanogr.,* **9,** 1183–1206.

Nof, D., 1985: Joint vortices, eastward propagating eddies and migratory Taylor columns. *J. Phys. Oceanogr.,* **15,** 1114–1137.

Paldor, N., and D. Nof, 1990: Linear instability of an anticyclonic vortex in a two-layer ocean. *J. Geophys. Res.,* **95,** 18 075–18 079.

Price, J. F., and H. T. Rossby, 1982: Observations of a barotropic planetary wave in the western North Atlantic. *J. Mar. Res.,* **41**(Suppl.), 543–558.

Qiu, B., 1990: Low-frequency shelf–slope responses induced by localized offshore forcings. *J. Geophys. Res.,* **95,** 9447–9459.

Ramp, S. R., 1989: Moored observations of current and temperature on the shelf and upper slope near Ring 82B. *J. Geophys. Res.,* **94,** 18 071–18 087.

Shaw, P.-T., and G. T. Csanady, 1983: Self-advection of density perturbations on a sloping continental shelf. *J. Phys. Oceanogr.,* **13,** 769–782.

——, and C.-Y. Peng, 1987: A numerical study of the propagation of topographic Rossby waves. *J. Phys. Oceanogr.,* **17,** 358–366.

——, and G. T. Csanady, 1988: Topographic waves over the continental slope. *J. Phys. Oceanogr.,* **18,** 813–822.

Smith, D. C., IV, 1986: A numerical study of Loop Current eddy interaction with topography in the western Gulf of Mexico. *J. Phys. Oceanogr.,* **16,** 1260–1272.

Thompson, R. O. R. Y., and J. Luyten, 1976: Evidence for bottom trapped topographic Rossby waves from single moorings. *Deep-Sea Res.,* **23,** 629–635.